Nanomed Res J 7(1):56-65, Winter 2022

RESEARCH ARTICLE

Raman Spectroscopy and Histopathology of Rat Bladder Cancer treated by Doxorubicin and Cisplatin using reduced graphene oxide as carrier

Wagner. J. Fávaro[1,*], Renata A. Villela[1], Helder J. Ceragioli[2], Nelson Durán[1,3]

[1] Laboratory of Urogenital Carcinogenesis and Immunotherapy, Biological Institute, Department of Structural and Functional Biology, University of Campinas, Campinas-SP, Brazil, 2FEEC, Department of Semiconductors, Instruments and Photonics, Electric and Computation Faculty, University of Campinas, Campinas-SP, Brazil, 3Nanomed Center, Federal University of ABC, Santo André, SP., Brazil

[2] Dr. Nelson Durán, Laboratory of Urogenital Carcinogenesis and Immunotherapy, Biological Institute, Department of Structural and Functional Biology, University of Campinas, Campinas-SP, Brazil

[3] Prof. Dr. Wagner. J. Fávaro- Laboratory of Urogenital Carcinogenesis and Immunotherapy, Biological Institute, Department of Structural and Functional Biology, University of Campinas, Campinas-SP, Brazil

ARTICLE INFO

Article History:
Received 05 October 2021
Accepted 20 December 2021
Published 01 January 2022

Keywords:
Reduced graphene oxide
bladder cancer
doxorubicin
cisplatin
Raman

ABSTRACT

Raman spectroscopy is a promising diagnostic technique used to identify different cancer types; however, few reports have correlated this information to histopathological analyses conducted in vivo or ex-vivo. It is well-known that using a set of techniques is important and necessary to get reliable and safer results. Identifying chemical changes in the Raman spectrum of healthy and pathological tissues enables better understanding the effects of treatments to be adopted, as well as optimizing pathological information and preventing cell death from taking place as slow biomolecule degradation of biomolecules. The treatment applied to non-muscle invasive bladder cancer (NMIBC) in the presence of reduced graphene oxide (rGO), rGO with cisplatin, rGO with doxorubicin, as well as the association of chemotherapeutics, such as rGO, with cisplatin and doxorubicin, followed by Raman spectroscopy and histopathological analyses, have shown the feasibility of using these two techniques to monitor NIMBC development in rats based on different chemotherapeutic formulations. Moreover, Raman tests have confirmed structural and biochemical changes in urinary bladder due to pathological process and exposure to chemotherapeutic agents.

How to cite this article
Fávaro W.J., Villela R.A., Ceragioli H.J., Durán N. Raman Spectroscopy and Histopathology of Rat Bladder Cancer treated by Doxorubicin and Cisplatin using reduced graphene oxide as carrier. Nanomed Res J, 2022; 7(1): 56-65. DOI: 10.22034/nmrj.2022.01.005

INTRODUCTION

Raman spectroscopy is capable of identifying biomolecular changes associated with cancer progression; thus, this technique can be used as non-invasive tool to help diagnosing bladder cancer. A literature review has followed the evolution of studies on this topic, from the first experiment conducted *in vitro* to the application of this technique *in vivo* near 2014. It identified how diagnostic algorithms were developed and provided molecular information correlated to the etiology of the biochemical continuum of cancer progression [1]. According to histopathologists, Raman spectroscopy has the potential to help identifying and classifying biochemical changes associated with carcinogenesis. Raman demonstrating also a rapid, reproducible and non-destructive tissue during the analyses of a specific composition [2].

Bladder samples were examined through Raman spectroscopy; analysis results have shown healthy tissues, carcinoma *in situ* (CIS), as well as low- (LGC), moderate- (MGC) and high-

* Corresponding Author Email: *nelsonduran1942@gmail.com*
wjfavaro@gmail.com

grade carcinoma (HGC), after routine cystoscopy [3]. The mean spectra observed for each group has demonstrated subtle differences; principal component analysis was used to divide the five pathology groups presented by the analyzed specimens as much as possible. Stone et al [3] have explained these differences as increasing malignancy grades and likely the hard task to fully differentiate these groups based on only histopathology.

Raman spectroscopy was capable of distinguishing non-tumor from tumor bladder tissues. The compact fiber probe-based imaging Raman (CFPBI) system was enabled to Cordero et al [4] to correctly classify these tissues with high sensitivity and high specificity. The Raman endoscopic system was applied to 107 tissue samples collected from patients with bladder cancer during transurethral tumor resection; spectra were analyzed based on multivariate statistical methods. Multivariate algorithm enabled differentiating non-malignant from malignant tissues at sensitivity and specificity of approximately 79%. The authors have suggested that, despite the small number of samples, data have shown great potential to identify bladder wall lesions during endoscopy [5,6].

Laser-based confocal Raman micro-spectroscopy and principal component analysis (PCA)/support vector machines were used to build diagnostic algorithms capable of determining histological diagnosis based on the leave-one-out cross validation of its Raman spectrum. Nucleic acid peak intensity of Raman spectra in bladder cancer cells and protein contents in healthy bladder cells have significantly increased. PCA and support vector machines (SVM) were effective tools capable of differentiating bladder cancer from healthy bladder tissues. Excellent specificity, sensitivity, positive and negative predictive values of ~73% for bladder cancer diagnosis were observed through leave-one-out cross validation [7]. Wang et al. [7] have suggested that PCA/SVM-based Raman spectroscopy applications have promising potential to be used in bladder cancer diagnosis.

A preliminary study applied low-resolution fiber-optic Raman sensing (LRFORS) system to assess the potentially of Raman spectroscopy to diagnose diverse bladder pathologies *ex vivo*. Spectra from 32 bladder specimens were classified into 3 groups based on histopathological analysis, such as: healthy bladder tissues, low-grade and high-grade bladder tumors. Results have shown the potential of this technique - which uses LRFORS system - to diagnose bladder cancer *in vivo* [8,9].

The most recent technique comprised the combination between OCT (optical coherence tomography) and RS (Raman spectroscopy) to improve the diagnosis of, as well as to differentiate, different bladder cancer stages and grades *ex vivo* by associating complementary data supplied by these two techniques. RS was performed upon the identification of degenerated tissue via OCT in order to define the molecular profile of it through point observations at suspected sites. OCT enabled clearly differentiating healthy from malignant tissues through tomogram inspection (71%) of tumor staging, from pTa to pT2, as well as over texture analysis and k-nearest neighbor categorization. RS provided 93% accuracy at the time to differentiate low- from high-grade lesions through PCA analysis, which was followed by k-nearest neighbor categorization. Data have evidenced the potentiality of a multi-modal strategy associated with OCT to be used for fast pre-selection and staging cancerous lesions, as well as of using RS to enhance the differentiation between low- and high-grade bladder cancer in a l3bel-free, non-destructive and non-invasive manner [10]. Most recently, a literature review has addressed the application of RS in breast cancer cases; it discussed its potential to analyze either tissues *ex-vivo* or liquid biopsy samples. Its potential to be used for applications *in vivo* in research about cancer, as well as for translational and clinical applications [11].

Therefore, the aim of the current research was to apply an exhaustive histopathological analysis based on RS to rats chemically induced to NMIBC in order to investigate its potential to be used for tissue featuring purposes [5, 12-14].

MATERIALS AND METHODS

Reduced graphene oxide synthesis

rGO (reduced graphene oxide was obtained and featured, as previously published [15,16]. Doxorubicin (DOX) and Cisplatin (CIS) were provided from LC Laboratories (*Woburn, EUA*) and LibbsFarmacêutica LTDA (*Embu, São Paulo, Brasil*), respectively.

rGO disperssion in Pluronic® F68

Dispersion of rGO was obtained by adding a proper quantity of rGo to 1% of Pluronic F68 in such away to find the final solution of 2 mg/mL of rGO based on ultrasonication bath application for 20 min.

CIS and DOX adhesion to rGO

In total, 0.2 mg of DOX was added to 0.2 mL of physiological solution. This mix was added with 1 mL of rGO dispersion (2 mg/mL). Subsequently, 1.0 mL of rGO dispersion (2mg/mL) was added to 0.2 mL of CIS (0.05 mg) and shacked for 2h.

Experiment conducted in vivo with rats

Thirty female of seven weeks old Fischer 344 rats were purchased in the Multidisciplinary Center for Biological Investigation (CEMIB) at University of Campinas (UNICAMP). Animal studies were accredited by the institutional Ethics Committee on Animal Research (**CEUA/ UNICAMP, protocol no. 3569-1**). Rats were anesthetized with 10% ketamine (60 mg/kg, i.m.; Vibra®, Roseira, SP, Brazil) and 2% xylazine (5 mg/kg, i.m.; Vibra®, Roseira, SP, Brazil) before they were subjected to intravesical catheterization performed with 22-gauge angiocatheter. Animals remained anesthetized for approximately 45 min after catheterization in order to eliminate spontaneous micturition. Control group – Group 1: five control animals were treated with 0.30 ml of 0.9% physiological saline, intraperitoneally (i.p.) administered once a week, for 14 successive weeks. NMIBC induction was carried out in 25 rats that intravesically received n-methyl-n-nitrosourea (MNU; 1.5 mg/kg, dissolved in 0.30 ml of 1 M sodium citrate, pH 6.0) every other week, for two months [14]. Two weeks after the last MNU dose, all rats were subjected to ultrasound examination in order to assess the incidence of tumors. Then, MNU-treated rats were further separated into five groups (n=5 per group): the Cancer+rGO group (Group 2) was treated with 2.0 mg/mL of rGO, i.p. administered once a week, for one month and a half successive weeks; the Cancer + rGO + CIS group (Group 3) was treated with 0.2 ml of rGO added with 0.05 mg cisplatin (CIS), i.p. administered and complexed in rGO dispersion (2 mg/mL) once a week, for one week and a half successive weeks; the Cancer+rGO+ DOXO group (Group 4) was treated with 0.2 ml of rGO added with 0.2 mg doxorubicin (DOXO), i.p. administered and complexed in rGO dispersion (2mg/mL) once a week, for one month and half successive weeks; the Cancer+rGO+CIS+ DOXO group (Group 5) was subjected to the same procedure as Groups 3, 4 and 5.

After treatment was over, all animals were euthanized and all the their urinary bladders were collected and analyzed by histopathological and Raman spectroscopy analyses.

Histopathological Analysis

Urinary bladder samples were collected from all rats and fixed in Bouin solution for 12 hs. Post-fixation process, tissues were washed in 70% ethanol and subjected to dehydration in an rising up series of alcohols. Subsequently, tissue fragments were diaphanized in xylene for 2 h and included in plastic polymers (*Paraplast Plus, ST. Louis, MO, USA*). Afterword, the materials were cut (thickness = 5 μm) in Leica RM 2165 rotary microtome (*Leica, Munich, Germany*), stained with hematoxylin-eosin and photographed in Zeiss Axiophot light microscope (*Zeiss, Munich, Germany*). Studied groups were characterized based on the consensus staging suggested by the World Health Organization/International Society of Urological Pathology [17,18].

Histopathological results were confronted to a proportion test. The divergence between the two proportions was subjected to proportion test at 1% type-I error.

Raman spectroscopy measurement
Measurements

The experiment was carried out at the Electrical Engineering and Computing School, Department of Semiconductors, Instruments and Photonics, in Unicamp. Urinary bladder fragments were frozen in liquid nitrogen and stored in frezeer at -80°C. Raman Scattering Spectroscopy (in Via Renishaw microscope, England) with infrared laser excitation λ = 785 nm and 20x magnification lens was used to analyze changes in the investigated samples and to find the Raman spectra. Samples were subjected to the same analysis conditions, the observation field was selected at random, as well as the representative of the sample spectrum.

RESULTS AND DISCUSSIONS

Macroscopic and Histopathological Analyses

Macroscopic changes were not observed in the peritoneum of the Control or Cancer group (**Fig. 1A**). However, animals in the Cancer + rGO group presented dark agglomerates in the peritoneum (**Fig. 1B**). It may have happened due to slow rGO compound absorption by mesenteric vessels when it was intraperitoneally (i.p.) administered.

This perspective has shown that GO and rGO administered via i.p. remained for more than a month in animals' body when PEG was used

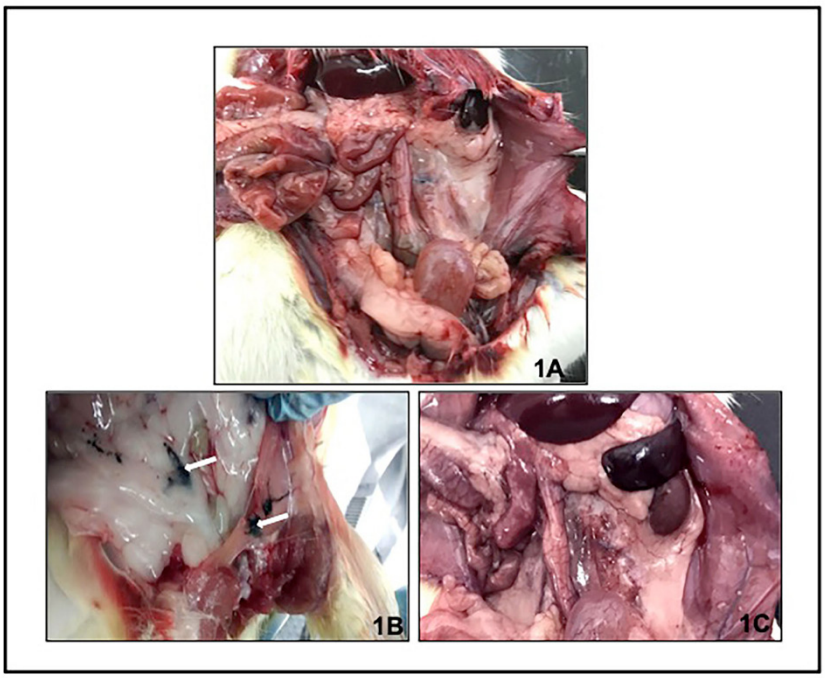

Fig 1: Exposure of abdominopelvic cavity in the animals from Cancer (A), rGO (B) and rGO+CIS or rGO+DOXO or rGO+CIS+DOXO (C). (A) and (C) Normal features of organs and peritoneum in the abdominopelvic cavity. (B) Presence of dark agglomerates (**arrows**).

as polymer in carbon nanotubes. Although this finding leads to concern about toxicity, no toxicity of graphene-based materials (GBMs) has been proven, so far [19]. Guo and Mei [19] have also reported that animals did not present damage in the main organs, although dark spots on the liver and spleen were observed - they subsided over time. The observed aggregate can lead to thrombus formation and, later on, it can lead to animals' death. In addition, GO-PEG i.p. administration has led to the presence of nanomaterial in animals' bodies for three months, and it evidenced that GBMs' behavior *in vivo* and toxicology depend on the administration route [20].

Dark agglomerates were not observed in the peritoneum of the herein investigated animals when CIS and/or DOXO were dispersed with rGO (**Fig. 1C**); this finding has indicated higher absorption of these compounds by mesenteric vessels. In addition, carbon nanotubes in contact with biological fluids have adsorbed biomolecules and formed their "corona" by reducing the surface energy of carbon nanotubes and by promoting its dispersion – this factor played important role in carbon nanotubes identification process [21].

With respect to histopathological results, the Control group did not show histological changes in bladder tissue (**Figs. 2a, 2b; Table 1**). Healthy bladder urothelium was composed of basal, intermediate and surface cell layers (umbrella cells) (**Figs. 2a, 2b**). On the other hand, all animals in the Cancer group have shown 100% malignant lesions, such as urothelial carcinoma with lamina propria invasion (pT1) (**Figs. 2c, 2d; Table 1**).

Urothelial papillary carcinoma (pTa) (**Figs. 2e, 2f**) and pT1 were the most frequent neoplastic lesions observed in the Cancer+rGO group – they affected 60% and 40% of rats, respectively (**Table 1**). Similarly, the Cancer+rGO+CIS group has shown 100% malignant lesions, such as pTa (**Figs. 2g, 2h**) and pT1 – these lesions affected 80% and 20% of rats, respectively (**Table 1**).

Rats in the rGO+DOXO group have shown malignant lesions, such as flat carcinoma *in situ* (pTis) (**Figs. 2i, 2j**) and pTa. These lesions affected 60% and 40% of rats, respectively (**Table 1**).

Animals treated with rGO+CIS+DOXO have clearly shown better histopathological recovery from cancer than those subjected to the other treatments – this group has shown decreased neoplastic bladder lesion progression in 40% of animals (**Table 1**). Benign lesions, such as flat hyperplasia (**Figs. 2k, 2l**), were found in 40% of rats in this group (**Table 1**). The most frequent

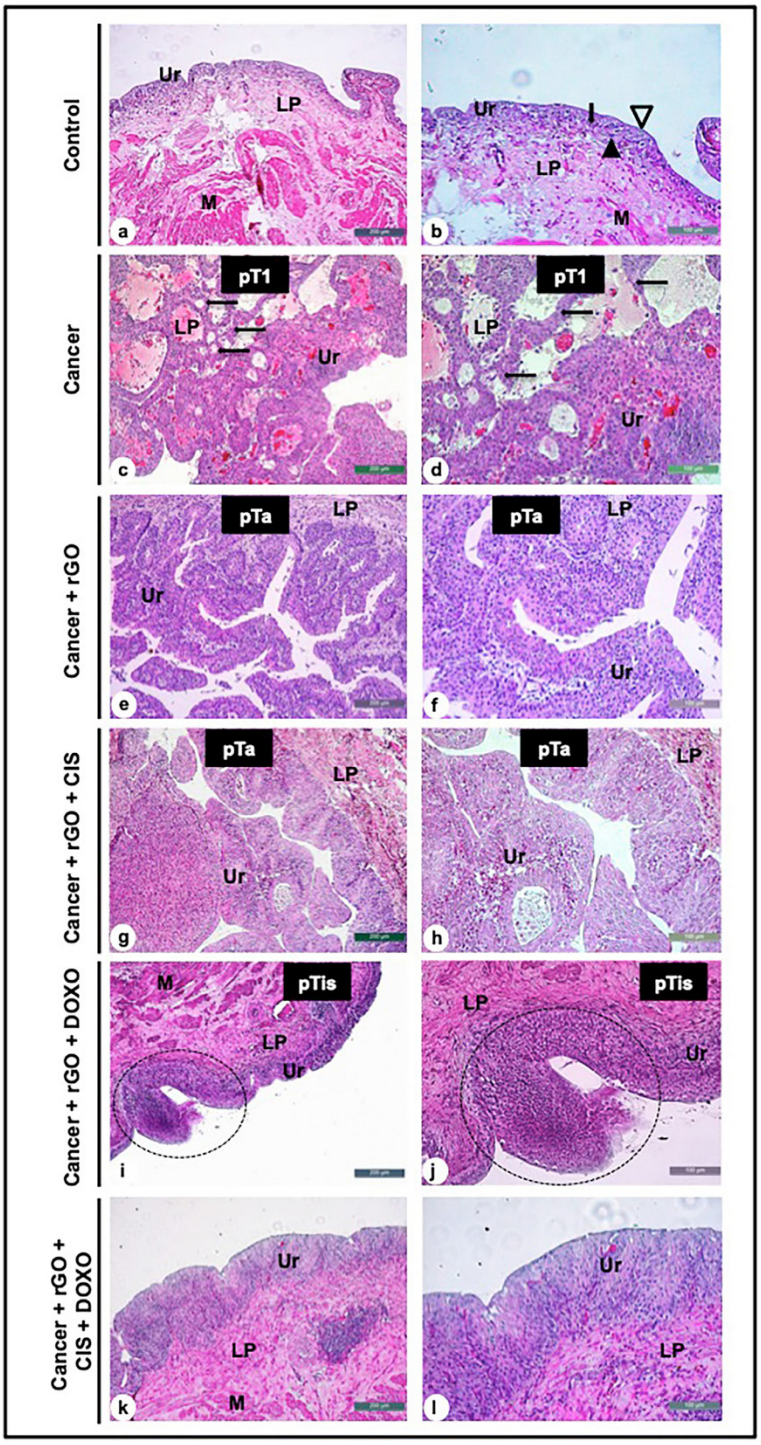

Fig 2: Representative photomicrographs of urinary bladder from Control (a, b), Cancer (c, d), Cancer + rGO (e, f), Cancer + rGO + CIS (g, h), Cancer + rGO + DOXO (i, j) and Cancer + rGO + CIS + DOXO (k, l) groups. (a), (b) Three different cell types composed the normal bladder urothelium: basal cell layer (**arrowhead**), intermediate cell layer (**arrow**) and surface cell layer (or umbrella cells, **open arrowhead**). (c), (d) pT1 tumor: cancer cells (**arrows**) invading the lamina propria. (e), (f), (g), (h) pTa tumor: cancer cells show slender papillae with frequent branching, minimal fusion, and variations in nuclear polarity, size, shape, and chromatin pattern and with the presence of nucleoli. (i), (j) pTis tumor: flat lesion (**circle**) in the urothelium surface characterized by large and pleomorphic cells, severe nuclear atypia and loss of cellular polarity. (k), (l) Flat hyperplasia characterized by thickening of the urothelium without cellular atypia. **a – l: Lp** – lamina propria, **M** – muscle layer, **Ur** – urothelium

Table 1. Histopathological alterations (%) in the urinary bladder in rats from different experimental groups.

Histopathology	Groups					
	Group 1 (*n=5*)	**Group 2 (*n=5*)**	**Group 3 (*n=5*)**	**Group 4 (*n=5*)**	**Group 5 (*n=5*)**	**Group 6 (*n=5*)**
Normal	05 (100%)*	-	-	-	-	-
Flat hyperplasia	-	-	-	-	-	02 (40%)*
Flat Carcinoma *in situ* (pTis)	-	-	-	-	03 (60%)*	02 (40%)
Urothelial papillary Carcinoma (pTa)	-	-	03 (60%)	04 (80%)*	02 (40%)	01 (20%)
Urothelial carcinoma with invasion of lamina propria (pT1)	-	05 (100%)*	02 (40%)	01 (20%)	-	-

Groups: Control (Group 1), Cancer (Group 2), Cancer+rGO (Group 3), Cancer+rGO+CIS (Group 4), Cancer+rGO+DOX (Group 5) and Cancer+rGO+CIS+DOX (Group 6). Benign lesions: Flat hyperplasia; Malignant lesions: pTis, pTa e pT1.
*$P<0.0001$ (proportions test).

neoplastic lesion found in this group was pTis, which affected 20% of rats (**Table 1**).

Raman spectroscopy.

The current study took into consideration bladders with lesions that were more representative of the analyzed groups of animals, as well as the treatment dispersions they were subjected to, which led to the spectra (**Fig. 3**), based on which, it was possible generating the table with the observed peaks (**Table 2**). According to reports, healthy bladder tissues have shown bands at 875; 1,080; 1,289; 1,303; 1,446 and 1,657 cm^{-1}, which are considered high and can be attributed to lipids and proteins [8]. On the other hand, bands observed in bladder cancer at 1,330; 1,462 and 1,662 cm^{-1}were associated with guanine, proteins and tryptophan, respectively [6]. Peaks observed for healthy tissues are often displaced (between 1 and 5 cm^{-1}) or missing in tumor tissues. It is worth emphasizing that detecting non-aromatic amino acids was a defying task, since they generate weak vibrational signals due to their poor polarity; but, aromatic amino acids present significant vibrational peaks due to the incidence of benzene ring. Nucleic acid peaks were observed through vibration in DNA bases, which are masked in healthy tissues. Cells proliferate without control; DNA amount significantly increases during malignant transformations - this process is followed by changes in phosphate, deoxyribose or bases [8]. The incidence of nucleic acids (~ 1,340 cm^{-1}) observed in the cancer group resulted from malignancy of the neoplastic process, which is basically a cellular process presenting high protein and lipid levels [22]. Protein visualization through Raman spectrum provides information about amino acid chains and that plays crucial role in interactions between protein structure and function [8].

Only peaks different from those presented in the control and cancer groups were taken into consideration at the time to observe nanocomposites' interaction in NMIBC treatment. The following peaks were observed in the rGO group: 930; 1,285; 1,770 and 2,958 cm^{-1}. Carbohydrate peaks at 930 cm^{-1} according to studies that the accumulation of the compound occurs during maturation and disappear with the loss of differentiation during neoplasia [23]. The 1,285 cm^{-1} band is associated with cytosine [24]; nucleic acid-associated peaks and DNA structure suggest the initiating of DNA fragmentation during apoptosis. The 1,770 cm^{-1} band is associated with vibration strength at C = O bond of δ lactone.

Peak in the rGo+CIS was observed at 1667 cm^{-1}, which referred to protein band, C = C band stretching, amide I helix structure and structural mode of tumor proteins. According to Chen et al [8] studies, bands representing proteins vary in cancer tissues, and it suggests weak interactions between chemical amino acid bonds in cancer cells. It happens because hydrogen bonds can be damaged and lead to protein structure loss or to alterations in the microenvironment of amino acid residues, in case of increased setting and unsetting of α-helix from β sheets [8].

The rGO+DOXO group presented the following peaks: 858; 1,259; 1,325; 1,667 and 2,953

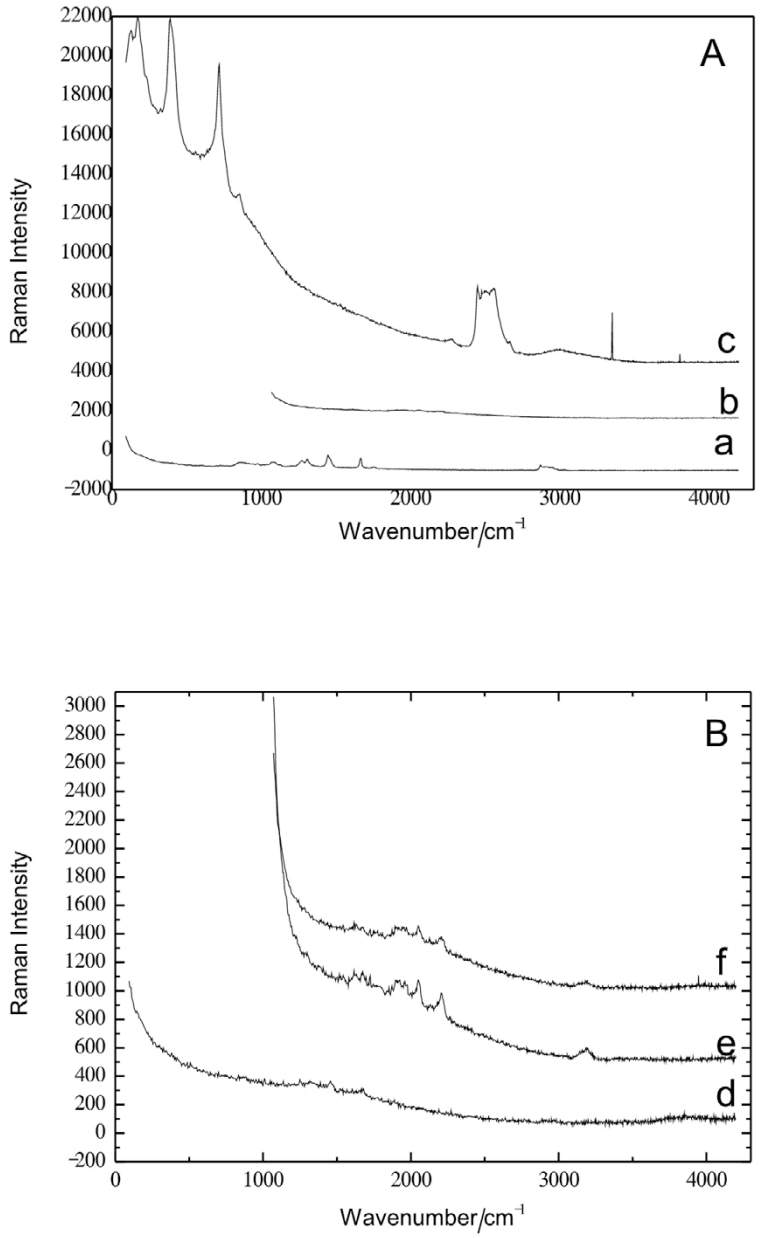

Fig 3: Typical Raman spectra from bladder of analyzed groups and the formulations of each treatment group submitted. Control (A), Cancer (B), treated group with rGO (C), treated group with rGO+CIS (D), treated group with rGO+DOXO (E), treated group with rGO+CIS+DOXO (F).

cm^{-1}. The peak at 858 cm^{-1} refers to tyrosine and collagen; increased DNA and decreased collagen levels are expected, since the core / cytoplasm ratio increases from healthy tissues to neoplastic ones. Cells become more abundant and the extracellular matrix, which presents abundant collagen amounts, reduces until the tumor gets bigger, and collagen I and III in the bladder become more abundant [3].

This process means that cancer cells produce and release matrix metalloproteinase in order to degrade the protein matrix, in the case of collagen, a fact that enables metastasis because the proliferation of cancer cells can mask the collagen signal in the matrix [8].

Table 2. Raman spectra analyses from urinary bladder: Control (Group 1), Cancer (Group 2), Cancer+rGO (Group 3), Cancer+rGO+-CIS (Group 4), Cancer+rGO+DOX (Group 5) and Cancer+rGO+CIS+DOX (Group 6).

Wavelenght (cm^{-1})						Peak Assignments	Ref.
Group 1	**Group 2**	**Group 3**	**Group 4**	**Group 5**	**Group 6**		
730						Phosphatidylserine (lipid)	Harvey et al., 2013
				858		Tyrosine, collagen	Movasaghi et al., 2007
866	863					Ribose vibration different mode than RNA (with 915 and 974 cm^{-1})	Movasaghi et al., 2007
		930				Carbohydrate peaks for solutions and solid	Movasaghi et al., 2007
976						Ribose vibration, different mode of RNA (with 874 and 915 cm^{-1})	Movasaghi et al., 2007
1086		1089				Gauche vibration (C-C)	Movasaghi et al., 2007
					1242	Amide III (β-sheet and random distribution)	Movasaghi et al., 2007
				1259		Cytosine (NH_2), guanine. Amide III	Movasaghi et al., 2007
1271						CHα rocking	Movasaghi et al., 2007
		1285				Cytosine	Movasaghi et al., 2007
1307		1308	1305			CH_3/CH_2 twisting or bending mode of lipid/ collagen	Movasaghi et al., 2007
				1325		CH_3CH_2 wagging mode present in collagen & purine bases of DNA	Movasaghi et al., 2007
					1328	Typical phospholipid	Movasaghi et al., 2007
	1333					Guanine	Movasaghi et al., 2007
1452		1452		1452		Protein bands . Umbrella mode of methoxyl . C-H bending mode of structural proteins	Movasaghi et al., 2007
					1457	Deoxyribose	Movasaghi et al., 2007
	1462		1461			CH_2, Disaccharides, sucrose, protein symmetric CH_2 and CH_3 deformation	Hu et al., 2013
	1549				1549	Tryptophan; tryptophan and /or β-sheet; tryptophan (IgG)	Hu et al., 2013
			1667	1667		Protein band, C=C stretching band, a-helical structure of amide, Structural protein modes of tumors. Carbonyl stretch (C=O)	Movasaghi et al., 2007
1669		1668				Carbonyl stretch (C=O), Cholesterol ester	Movasaghi et al., 2007
1758						One of absorption positions for the C=O stretching vibrations of cortisone	Movasaghi et al., 2007
		1770				ϒ-lactone	Parker, 1983
2870		2873				CH_2 symmetric stretch of lipids & CH_2 asymmetric stretch of lipids and proteins	Movasaghi et al., 2007
		2907				CH stretch	Movasaghi et al., 2007
2925						Symmetric CH_3 stretch. Due primarily to protein	Movasaghi et al., 2007
					2951	CH_3 asymmetric stretch	Movasaghi et al., 2007
				2953		CH_3 asymmetric stretch	Movasaghi et al., 2007
		2958				Probably CH_2 asymmetric vibration	Zou et al., 2015

In special, the phenyl peak at 1,005 cm^{-1} and the protein C–H deformation and adenine, guanine nucleic acid peak at 1,342 cm^{-1} presented sharp intensity diminishes for all but one cell at 48 h time points, doing these excellent biomarkers of cell death [24]. In 1,640 cm^{-1} protein band stretching of the band C = C α-amide structure of the amide I structural mode of tumor proteins [25].The 2,953 cm^{-1} band, which refers to asymmetric CH_3 elongation, has shown that Raman spectroscopy was capable of differentiating CH_3 from CH and CH_2CH_3, which have the same features in the spectrum.

Changes in the optical properties of tissues, such as increased urothelium thickness, as well as morphological changes (increased cell density), can mitigate excited light penetration, and decrease the amount of photons emitted in the stromal region of neoplastic tissues in comparison to that of healthy tissues [26].

The following peaks were observed in the rGo+CIS+DOXO group: 1,242; 1,328 1,457 and 2,951 cm^{-1}. Peak 1,242 cm^{-1} represents amide III (β sheet and random distribution were attributed to amide III vibrations, in both of protein structure such as elastin and collagen [27]. The 1,328 cm^{-1} band has shown typical phospholipids [21]; "healthy" tissues were rich in lipids, which were uniformly distributed, whereas tumor tissues were more concentrated and evident. The 1,457 cm^{-1} band corresponds to deoxyribose and at 2,951 cm^{-1}appeared the asymmetric stretch of CH_3.

Bands ranging from 1,230 to 1,300 cm^{-1} refer to lipids and proteins [6] that derive from the lamina propria and muscular layer in healthy bladder tissues. According to reports, lipid peaks were mainly generated due to cell membrane vibration, C-H and C-C bonds of lipids and C = C unsaturated fatty acids. Peaks associated with amino compound III were mainly produced by C-N elongation vibration and N-H binding vibration, which indicated presence of protein in the β-sheet structure [9].

These changes are associated with disease progression, since bladder tumors are often papillary and quite vascular, and they do not penetrate necrotic sites [3]. Identifying chemical changes in the Raman spectrum of healthy and pathological tissues enables better understanding the effects of treatments, as well as allows optimizing pathological information. Moreover, cell death does not take place as a slow biomolecule degradation process [28], but as a singular fast event[2]. Raman spectroscopy allowed the first approximation between biochemical bases to help better understanding the pathological process of carcinogenesis [3].

The techniques herein adopted to feature the rGO sample were very useful, since they were capable of providing data that confirmed the nature of this compound. Using a set of techniques was essential and necessary to help finding reliable and safer results. The rGO tests conducted *in vivo* did not show significant toxicity; rGO sheets in the group subjected to the combination between CIS and DOXO chemotherapy complexes had positive effects on NMIBC therapy in comparison to the groups treated with isolated chemotherapeutic agents. Raman tests have confirmed structural and biochemical changes in rats' urinary bladder due to pathological process and to their exposure to chemotherapeutic agents.

CONCLUSIONS

At the end of the activities developed and in light of the objectives outlined in the conception of this study, it can be concluded that:

All of the techniques employed in the characterization of the rGO sample proved to be very useful, providing data that confirmed the nature of the compound. The use of a set of techniques has proven to be of importance and necessary to obtain reliable and safer results; in the in vivo tests rGO did not present significant toxicity and the group with combination of the CIS and DOXO chemotherapy complexes the rGO sheets presented positive effects against the NMIBC therapy when compared to the groups with isolated chemotherapeutic agents; Raman tests confirm structural and biochemical changes in the urinary bladder due to the pathological process and exposure to chemotherapeutic agents.

ACKNOWLEDGEMENTS

Support from FAPESP, CNPq, NanoBioss (MCTI), INOMAT (MCTI/CNPq) and Prof. Dr. Hudson Zanin/FEEC/Unicamp-Brazil for the Raman equipment .

CONFLICT OF INTEREST

The authors declare no conflicts of interest.

REFERENCES

1. Kerr LT, Domijan K, Cullen I, Hennelly BM. Applications of

Raman spectroscopy to the urinary bladder for cancer diagnostics. Photonics & Lasers in Medicine. 2014;3(3).
2. Kallaway C, Almond LM, Barr H, Wood J, Hutchings J, Kendall C, et al. Advances in the clinical application of Raman spectroscopy for cancer diagnostics. Photodiagnosis and Photodynamic Therapy. 2013;10(3):207-19.
3. Stone N, Hart Prieto MC, Crow P, Uff J, Ritchie AW. The use of Raman spectroscopy to provide an estimation of the gross biochemistry associated with urological pathologies. Analytical and Bioanalytical Chemistry. 2006;387(5):1657-68.
4. Cordero E, Rüger J, Marti D, Mondol AS, Hasselager T, Mogensen K, et al. Bladder tissue characterization using probe-based Raman spectroscopy: Evaluation of tissue heterogeneity and influence on the model prediction. Journal of biophotonics. 2020;13(2):e201960025-e.
5. Grimbergen MCM, van Swol CFP, Draga ROP, van Diest P, Verdaasdonk RM, Stone N, et al. Bladder cancer diagnosis during cystoscopy using Raman spectroscopy. SPIE Proceedings; 2009/02/12: SPIE; 2009.
6. Draga ROP, Grimbergen MCM, Vijverberg PLM, Swol CFPv, Jonges TGN, Kummer JA, et al. In Vivo Bladder Cancer Diagnosis by High-Volume Raman Spectroscopy. Analytical Chemistry. 2010;82(14):5993-9.
7. Wang L, Fan J-H, Guan Z-F, Liu Y, Zeng J, He D-L, et al, Study on bladder cancer tissues with Raman spectroscopy. Guang Pu Xue Yu Guang Pu Fen Xi. 2012; 32:123-126.
8. Chen Y, Dai J, Zhou X, Liu Y, Zhang W, Peng G. Raman spectroscopy analysis of the biochemical characteristics of molecules associated with the malignant transformation of gastric mucosa. PLoS One. 2014;9(4):e93906-e.
9. Chen H, Li X, Broderick N, Liu Y, Zhou Y, Han J, et al. Identification and characterization of bladder cancer by low-resolution fiber-optic Raman spectroscopy. Journal of Biophotonics. 2018;11(9):e201800016.
10. Bovenkamp D, Sentosa R, Rank E, Erkkilä M, Placzek F, Püls J, et al. Combination of High-Resolution Optical Coherence Tomography and Raman Spectroscopy for Improved Staging and Grading in Bladder Cancer. Applied Sciences. 2018;8(12):2371.
11. Hanna K, Krzoska E, Shaaban AM, Muirhead D, Abu-Eid R, Speirs V. Raman spectroscopy: current applications in breast cancer diagnosis, challenges and future prospects. Br J Cancer. 2021:1-15.
12. Fávaro WJ, Billis A, Nunes IS, Durán N. New immunotherapy for non-muscle invasive bladder cancer (NMIBC): effects of immunomodulator P-MAPA. Jlournal of Urology. 2012; 187 (Supl.): e231.
13. Garcia PV, Apolinário LM, Böckelmann PK, Nunes IS, Durán N, Fávaro WJ. Alterations in ubiquitin ligase Siah-2 and its corepressor N-CoR after P-MAPA immunotherapy and anti-androgen therapy: new therapeutic opportunities for non-muscle invasive bladder cancer. International Journal of Clinical and Experimental Pathology. 2015; 8: 4427-43.
14. Garcia PV, Seiva FRF, Carniato AP, de Mello Júnior W, Duran N, Macedo AM, et al. Increased toll-like receptors and p53 levels regulate apoptosis and angiogenesis in non-muscle invasive bladder cancer: mechanism of action of P-MAPA biological response modifier. BMC Cancer. 2016;16:422-.
15. Durán N, Villela RA Marcato PD, Garcia PV, Ceragioli HJ, Favaro WJ. *In vivo* evaluation of doxorubicin loaded in r-graphene oxide in bladder cancer model. Nano-2014 Conference, pp. 08.004. Moscow, Russia. 2014; 12: 144.
16. Zanin H, Saito E, Ceragioli HJ, Baranauskas V, Corat EJ. Reduced graphene oxide and vertically aligned carbon nanotubes superhydrophilic films for supercapacitors devices. Materials Research Bulletin. 2014;49:487-93.
17. Fávaro WJ, Nunes OS, Seiva FR, Nunes IS, Woolhiser LK, Durán N, et al. Effects of P-MAPA Immunomodulator on Toll-Like Receptors and p53: Potential Therapeutic Strategies for Infectious Diseases and Cancer. Infect Agent Cancer. 2012;7(1):14-.
18. Epstein JL, Amin MB, Reuter VR. The World Health Organization / International Society of Urological Pathology consensus classification of urothelial (tranticional cell) neoplasms of the urinary bladder. Bladder Consensus Conference Committee. The American Journal of Surgical Pathology. 1998; 22: 1435-48.
19. Chong Y, Ma Y, Shen H, Tu X, Zhou X, Xu J, et al. The in vitro and in vivo toxicity of graphene quantum dots. Biomaterials. 2014;35(19):5041-8.
20. Guo X, Mei N. Assessment of the toxic potential of graphene family nanomaterials. J Food Drug Anal. 2014;22(1):105-15.
21. Perez-Potti A, Lopez H, Pelaz B, Abdelmonem A, Soliman MG, Schoen I, et al. In depth characterisation of the biomolecular coronas of polymer coated inorganic nanoparticles with differential centrifugal sedimentation. Sci Rep. 2021;11(1):6443-.
22. Hu C, Wang J, Zheng C, Xu S, Zhang H, Liang Y, et al. Raman spectra exploring breast tissues: Comparison of principal component analysis and support vector machine-recursive feature elimination. Medical Physics. 2013;40(6Part1):063501.
23. Kamemoto LE, Misra AK, Sharma SK, Goodman MT, Luk H, Dykes AC, et al. Near-infrared micro-Raman spectroscopy for in vitro detection of cervical cancer. Appl Spectrosc. 2010;64(3):255-61.
24. Buckmaster R, Asphahani F, Thein M, Xu J, Zhang M. Detection of drug-induced cellular changes using confocal Raman spectroscopy on patterned single-cell biosensors. The Analyst. 2009;134(7):1440-6.
25. Wang J, Zheng C-X, Ma C-L, Zheng X-X, Lv X-Y, Lv G-D, et al. Raman spectroscopic study of cervical precancerous lesions and cervical cancer. Lasers Med Sci. 2021;36(9):1855-64.
26. Mo J, Zheng W, Low JJH, Ng J, Ilancheran A, Huang Z. High Wavenumber Raman Spectroscopy for in Vivo Detection of Cervical Dysplasia. Analytical Chemistry. 2009;81(21):8908-15.
27. Majka Z, Czamara K, Wegrzyn P, Litwinowicz R, Janus J, Chlopicki S, et al. A new approach to study human perivascular adipose tissue of the internal mammary artery by fiber-optic Raman spectroscopy supported by spectral modelling. The Analyst. 2021;146(1):270-6.
28. Li L, Mustahsan VM, He G, Tavernier FB, Singh G, Boyce BF, et al. Classification of Soft Tissue Sarcoma Specimens with Raman Spectroscopy as Smart Sensing Technology. Cyborg and Bionic Systems. 2021;2021:1-12.